




Short Communication

Influences of Atmospheric Humidity on Sliding Speed Characteristics of Dry Sliding Phenomena

Wei Chee Hong¹⁾, Kanao Fukuda ^{1,2)*} and Shahira Liza¹⁾

¹⁾ Malaysia-Japan International Institute of Technology, Universiti Teknologi Malaysia,
Jalan Sultan Yahya Petra, 54100 Kuala Lumpur, Malaysia

²⁾ International Research Center for Hydrogen Energy, Kyushu University,
744 Motoooka, Nishi-ku, Fukuoka 819-0395, Japan

*Corresponding author: Kanao Fukuda (fukuda.kl@utm.my)

Manuscript received 30 May 2023; accepted 09 August 2023; published 31 October 2023

Presented at the 9th International Tribology Conference, Fukuoka 2023, 25-30 September, 2023

Abstract

The effect of adsorbed water layers in sliding phenomena has been widely recognized, but it has yet to be explained thoroughly after many years of research. Previous researches tend to explain the phenomena from chemical and qualitative viewpoints, thus physical viewpoint approaches with quantitative evidence are necessary to complement the previous research works. Studies were done to estimate the thickness of adsorbed water layers in recent years to obtain quantitative evidence of the effect of adsorbed water layers. It was found that the thickness of the adsorbed water layer derived from atmospheric humidity could provide physical influences on sliding phenomena. The hypothesis in this study based on the Stribeck curve is; the friction coefficient may decrease significantly with the increase of sliding speed at high relative humidity (RH) compared to low RH. To verify the hypothesis, a pair of JIS SUS304 austenitic stainless steel balls were scratched against each other horizontally with a vertical overlapping distance of 80 μm at sliding speeds of 20, 200, and 2000 $\mu\text{m}\cdot\text{s}^{-1}$ in RH of 5, 55, and 95%. The experimental results supported the hypothesis as the friction coefficient for medium to high RH decreased significantly with increasing sliding speed while the friction coefficient decreases slightly at low RH. The friction coefficient decreases significantly at high sliding speed and RH. The possible physical effects of the adsorbed water layers were suggested.

Keywords

friction, sliding speed, adsorbed water, relative humidity, boundary lubrication, dry sliding, austenitic stainless steel

1 Introduction

It is well-known that relative humidity (RH) in the atmosphere significantly influences the sliding phenomena, especially in non-lubricated sliding. The RH forms adsorbed water layer on most surfaces especially metallic surfaces, which then affects the friction and wear during sliding. However, a lot of work is still needed to fully understand the mechanisms of sliding phenomena, due to the involvement of various disciplines and numerous variables, with each variable exerting an influence on the others. Several studies have been done to explain the role of RH in tribological phenomena, but these explanations have been limited to a qualitative chemical perspective, oxidation, and tribochemical reactions [1-5]. Other than chemical influences, physical influences such as the physical separation of surfaces by the adsorbed water layer also play an important role in the sliding phenomena [6-8]. Although there are studies that explored the physical effects of

the adsorbed water layer, more quantitative analyses are still needed [9-11]. Nano-scale studies have been more quantitative, focusing on the capillary effect on asperity adhesion [12-14], but it is not yet feasible to directly apply these findings to macroscopic phenomena. Therefore, previous research has not provided enough explanations or quantitative evidence for the effects of the adsorbed water layer, especially from a physical viewpoint.

The research group by the current authors aimed to obtain quantitative data on the effect of RH and the adsorbed water layer in sliding phenomena. They initially focused on investigating the early stages of sliding in metallic materials using a pin-on-disc setup to simplify the analysis [15-18]. For example, when studying the sliding of SUS 316, it was observed that at a moderate RH of 49%, severe adhesion occurred earlier compared to low and high RH [15]. This observation led to the suggestion that the meniscus effect of adsorbed water within this RH range enhances the adhesion of metallic surfaces.

By employing similar experimental conditions with varying applied loads, the authors discovered that severe adhesion starts earliest when a low applied load is combined with high RH [17]. The adsorbed water at different RH levels and applied loads exhibited different mechanisms that influenced friction and wear of materials. To investigate even earlier stages of sliding, the research group conducted ball-to-ball sliding tests [19-22]. Interestingly, they observed that the sliding friction during downhill motion was considerably higher than during uphill motion at different RH levels. The hypothesis put forward to explain these results was that RH contributes to the Laplace pressure within the water meniscus formed by the adsorbed water layer, resulting in unusually high lateral forces during specimen detachment. To further validate the physical effect of the adsorbed water layer in these peculiar observations, the tribological behavior of hydrophobic and hydrophilic materials was compared under different RH conditions [23]. In this experiment, PTFE samples did not exhibit any abnormal lateral force readings, whereas austenitic stainless steel samples consistently reproduced the peculiar phenomenon across all RH levels. These results were attributed to the physical effect of the adsorbed water layer on the sliding behavior of metallic surfaces. Although these findings seem to support the notion of Laplace pressure playing a role in the observed phenomenon, doubts remain regarding the dominant mechanism underlying the physical effect of the adsorbed water layer in generating these peculiar phenomena. In addition, the research group also conducted quantitative studies on the adsorbed water layer influenced by RH [24, 25]. The results showed that both RH and surface roughness directly impact the amount of adsorbed water on the sliding surfaces. Rougher surfaces tend to have more adsorbed water and require a longer time to reach the saturation point of the adsorbed water layer. Based on these results, it was found that the equivalent thickness of the adsorbed water layer, assuming that the surface has no crystallographic defects, can reach up to 60 nm, which is comparable to the surface

roughness of a specimen with a mirror finish. Furthermore, the drying time, which is defined as the time necessary to reach the saturation point when RH was changed from high value to low value, of the specimen is significantly longer than the wetting time, which is defined oppositely to the above and usually takes around 30 minutes [24]. These quantitative findings provide evidence that the thickness of the adsorbed water layer resulting from RH could induce mechanical or physical effects in macroscopic sliding phenomena.

Based on the previous studies, suggestions were made to carry out more quantitative studies on the physical influences of adsorbed water layers in sliding phenomena, by investigating the combined effect of adsorbed water layer and other physical manipulated variables, such as sliding speed. The hypothesis was made based on the Stribeck curve: at high RH, the friction coefficient will significantly decrease with increasing sliding speed and the sufficiently thick adsorbed water layer could induce dry to boundary lubrication; while at low RH, increasing the sliding speed will only slightly decrease the friction coefficient due to insufficient adsorbed water layer. To verify the hypothesis, ball-to-ball scratch tests were carried out to examine the friction coefficient variation with sliding speed at different RH levels and to discuss the potential physical effect of adsorbed water layer in sliding phenomena.

2 Experimental methods

2.1 Experiment equipment

The experiment involves the use of a ball-on-ball tribotester constructed by the research group shown in Fig. 1. The tribotester was designed and built to observe the initial contact of the protrusions on the sliding surfaces. This feature is essential to observe the physical effects of the adsorbed water layers in sliding phenomena. On the upper specimen lever, two load cells were used to determine the lateral force L and loading force W , and a laser displacement sensor was

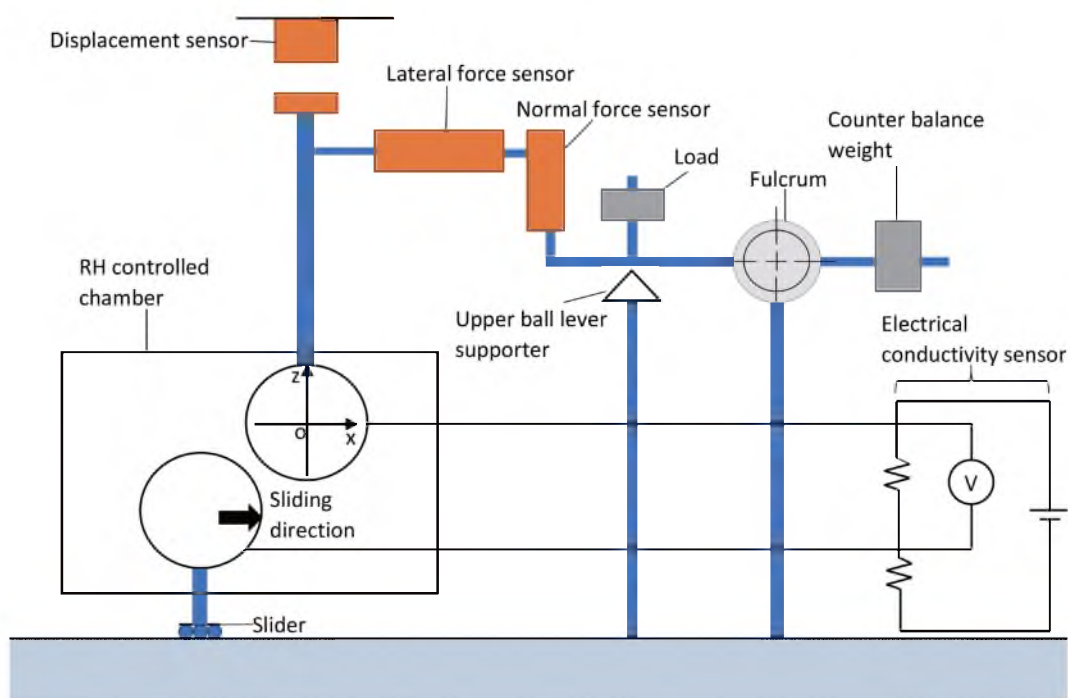


Fig. 1 Schematic drawing of ball-on-ball tribo-tester

employed to gauge the vertical displacement d of the upper specimen ball. The lever is supported by a fulcrum and pneumatic supporter. When there is no applied load, the lever is balanced by adjusting the position of the counterbalance weight. An electrical voltage V of 140 mV was applied between the specimens to assess the electrical resistance R at the sliding interface. The main component to control the sliding speed is a linear servo actuator with a speed rating of 2 to 6000 $\mu\text{m}\cdot\text{s}^{-1}$ connected to the lower ball specimen holder. To control the RH, an air humidifier that can regulate the RH from 3 to 98% and a maximum flow rate of 8 $\text{L}\cdot\text{min}^{-1}$ is linked to a partially confined chamber that contains the specimens. All the data readings were measured simultaneously with the sliding test using a data acquisition system [26, 27] with a spatial resolution of 5 μm along the x-axis.

The tester functions by sliding the lower ball specimen O' in the x-axis towards a stationarily fixed upper ball specimen O . There is a controlled vertical overlapping distance between the specimens in the z-axis, denoted as δ . For a complete unidirectional sliding cycle, the lower ball specimen approaches the upper ball specimen at a constant speed v . Upon contact with both specimens, the upper ball specimen is pushed up and down during the sliding process until the lower ball specimen detaches (Fig. 2).

2.2 Calculation of friction coefficient

The friction coefficient is calculated using the measured lateral force and loading force from the sliding test. The equilibrium formulae are referenced from the related previous study [23] listed as:

$$\alpha = \sin^{-1}\left(\frac{l}{D}\right) \quad (1)$$

$$F_f = L \cos \alpha - W \sin \alpha \quad (2)$$

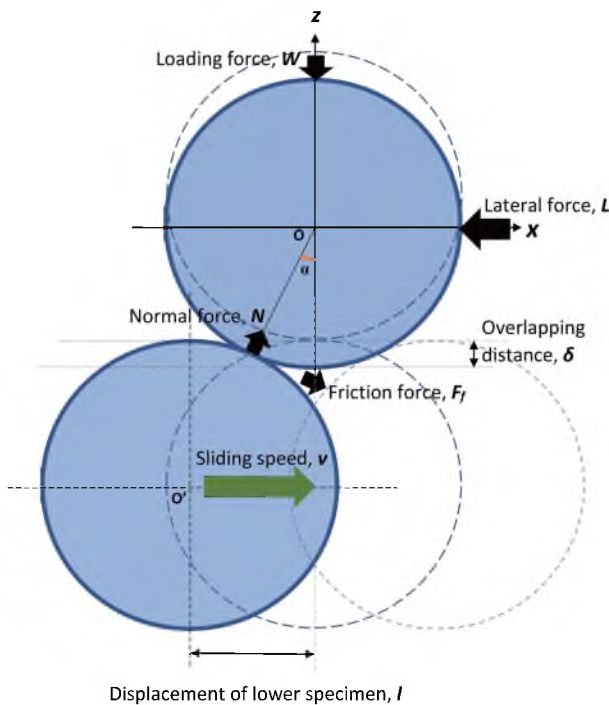


Fig. 2 Expected movement of the specimen balls and the forces exerted on the upper ball

$$N = W \cos \alpha + L \sin \alpha \quad (3)$$

$$\mu = \frac{F_f}{N} \quad (4)$$

Where F_f is the friction force, N is the normal force, l is the displacement of the lower specimen center O' from center O during sliding, D is the diameter of the specimen and μ is the friction coefficient. The formulae can be derived by referring to Fig. 2.

2.3 Specimen preparation

Before the sliding test, the specimens were polished to avoid surface contaminants and minor damage. To achieve this, the surface of each specimen was ground with 2000 grid sandpapers to remove any surface contamination and oxide layer and then polished using 0.1 μm diamond slurry. All specimens were maintained at an average surface roughness of less than 0.05 μm Ra to ensure consistency throughout the experiment. Following polishing, the specimens were ultrasonically cleaned in a 50:50 hexane-acetone mixture for 15 minutes and then dried for an additional 15 minutes using a hot plate set at 100°C. The RH in the confined chamber was controlled using an air humidity controller at an airflow rate of 2.5 $\text{L}\cdot\text{min}^{-1}$. The air humidity controller was allowed to run for 30 minutes before commencing the sliding test to ensure saturation of the adsorbed water on the specimen [24]. The procedures were repeated three times using new specimens to assess the repeatability of the results.

2.4 Experiment variables

In this experiment, the independent variables being manipulated are the sliding speed, set at 20, 200, and 2000 $\mu\text{m}\cdot\text{s}^{-1}$, and the RH, set at 5, 55, and 95%. The fixed independent variables include the surrounding temperature, maintained at 26°C, atmospheric pressure set at 1 atm, a fixed load of 10 N, and an overlapping distance of ball specimens δ set at 80 μm . The sliding test was conducted using two austenitic stainless steel balls with a diameter D of 8 mm as the sliding pair. Since this study focuses on the physical viewpoint, JIS SUS 304 was selected due to its good chemical resistance. Throughout the experiment, the monitored dependent variables were the lateral force L , loading force W , vertical displacement of the upper ball d , and the electrical resistance between the specimens R , all of which were monitored and recorded.

2.5 Hertzian contact

Before the experiment, the contact conditions of the specimen were evaluated using the Hertzian contact theory. Young's modulus and Poisson's ratio of JIS SUS 304 were estimated at 193 GPa and 0.29, respectively, based on various sources. With a 10 N load, the calculated radius of the area in contact, depth of indentation resulting from elastic deformation, and maximum contact pressure were 52.2 μm , 1.3 μm , and 1.75 GPa, respectively. As the calculated maximum contact pressure was lower than the measured hardness of the ball specimen which was 2.1 GPa, it was expected that the specimens would not undergo plastic deformation during the initial contact.

2.6 Adsorbed water layer thickness estimation

The thickness of the adsorbed water layer on austenitic stainless steel is reported as approximately 1.76, 14, and 19 nm at 5, 55, and 95% RH respectively [24]. For 0.04 μm R_q , the

maximum λ value (the ratio of liquid film thickness h to surface roughness Rq) are 0.044, 0.35, and 0.475 at RH 5, 55, and 95% respectively. At 5% RH, dry sliding phenomena are expected due to the adsorbed water layer growing in an ice-like network before reaching 30% RH. Thus, the friction coefficient at 5% RH would be high since the ice-like water structure cannot provide effective fluid-base lubrication. Since the thickness of adsorbed water layers is significantly thicker, the friction coefficient for 55% RH is expected to be slightly lower compared to 5% RH. On the other hand, at 95% RH, the adsorbed water layer is much thicker and mainly composed of a liquid structure, which might enable dry to boundary lubrication as the sliding speed increases.

2.7 Sliding system deformation compensation

The sliding system will undergo some elastic deformation due to the lateral force during sliding. The displacement due to the deformation will affect the sliding distance and measurement position of the responding variables, the actual movement of the specimen is illustrated in Fig. 3. To compensate for the deformed measurement, the elastic deformation of the sliding system was measured using a simple pulley system as illustrated in Fig. 4. A weight is connected to the specimen holder, supported by a stand and bearing pulley. The laser displacement sensor is placed horizontally and aimed toward the center of the specimen holder. The weight is attached as close as possible to the center of the specimen to obtain a more precise displacement. Weights ranging from 5 to 20 N were used for the measurement, gradually increased by 5 N, and then decreased to check the hysteresis of the system.

3 Results and discussion

3.1 Sliding system deformation compensation

Figure 5 shows the elastic deformation of the sliding system at the x-axis for both the upper and lower specimen holder.

Some slight hysteresis is observed for the upper specimen holder, and the maximum displacement could reach up to 420 μm with a 20 N load. In comparison, the elastic deformation in the lower specimen holder is almost negligible, both increasing and decreasing load show a very linear pattern. Using these results, the estimated trend equation of the system displacement dx is obtained as:

$$dx = -0.0289 W_x^3 + 0.8641 W_x^2 + 15.79 W_x \tag{5}$$

Where W_x is the horizontal load applied on the specimen holder. By substituting L as W_x , the measured travel distance is adjusted to compensate for the extra displacement caused by the elastic deformation of the sliding system. The raw measurement and the exact relative positions of the variable after the displacement compensation are included in Fig. 6 for comparison. To avoid confusion, the discontinuity of the compensated plot is due to the ‘jumped’ data after the compensation of the displacement due to the high lateral force, there are no actual data recorded in this region.

3.2 Result repeatability and reliability

To confirm the repeatability of the results, the experiment procedures are repeated at least three times for each sliding condition. The results for the same parameters are compared to observe the general trend of the variables, then one of the moderate results among the similar trend and magnitude is selected for analysis. To clarify the selection of the data, the comparison of friction coefficient for all sliding tests for 2000 $\mu\text{m}\cdot\text{s}^{-1}$ at all RH is used as the representative of the repeatability results, shown in Fig. 7. The results show good repeatability with a similar trend for 5 and 95% RH. Among the 3 tests for 55% RH, test 1 shows an unreasonable low magnitude with a fairly similar trend as tests 2 and 3, thus test 4 was done for further confirmation. The outlier for test 1 might be caused by the inevitable presence of contaminants on the specimen

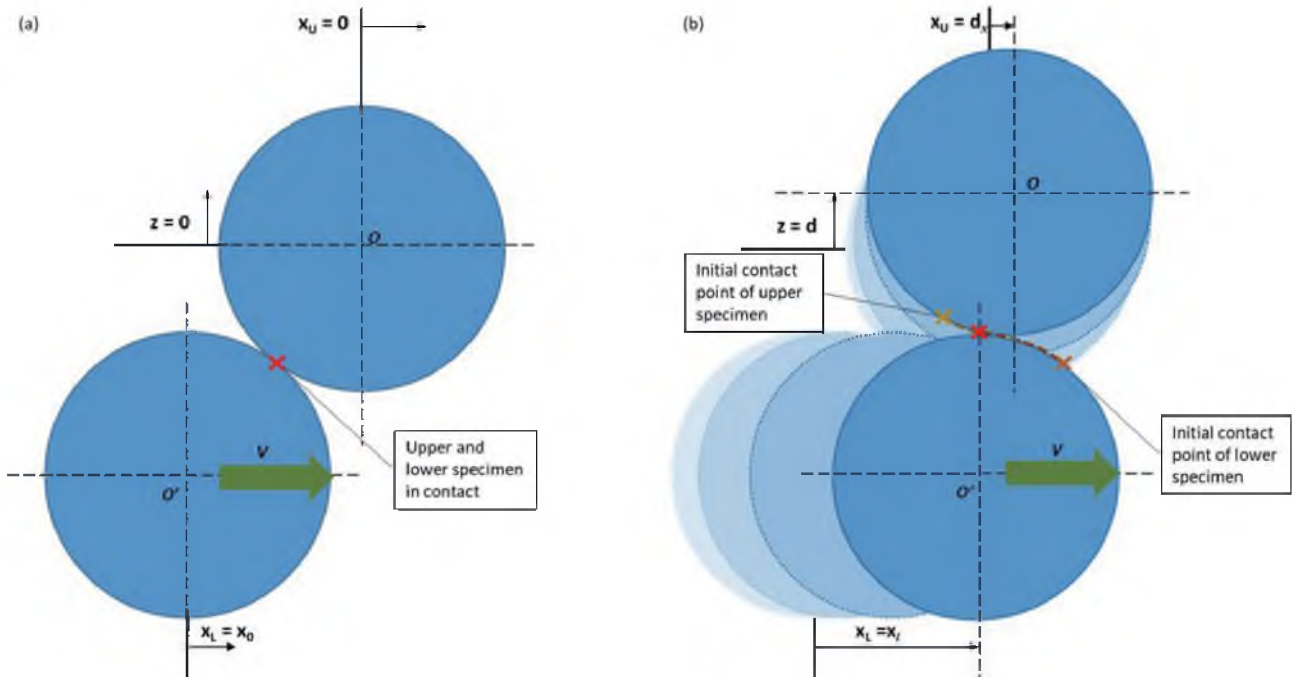


Fig. 3 Actual position of the sliding specimens (a) at initial contact ($x \approx 700 \mu\text{m}$) and (b) during sliding reaching the middle point ($x \approx 2000 \mu\text{m}$)

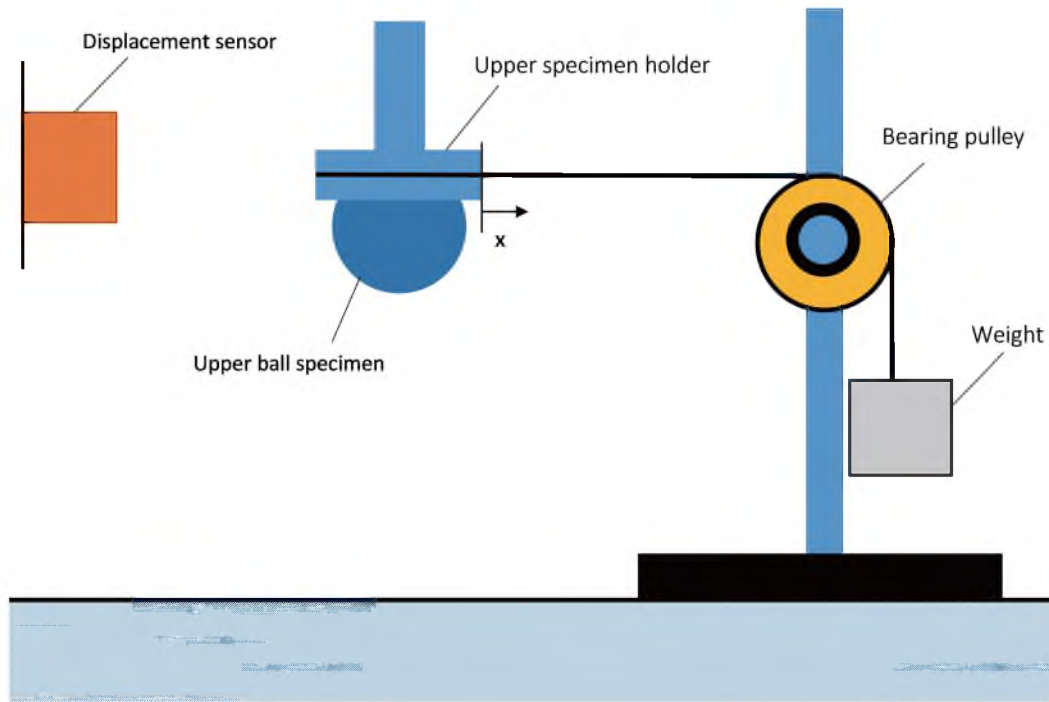


Fig. 4 Simple pulley system to measure the system elastic deformation of the upper specimen holder

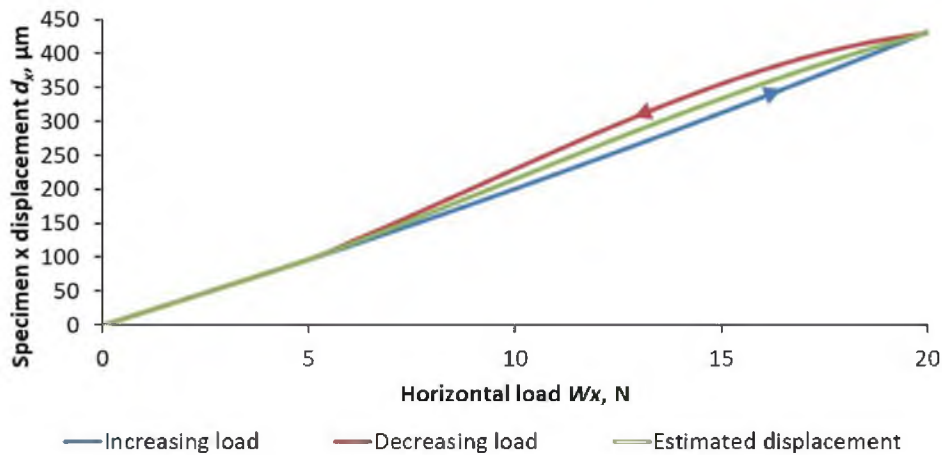


Fig. 5 Specimen holder x-displacement due to system deformation for increasing and decreasing load

surfaces during the drying process before the sliding test.

3.3 Lateral force, loading force, vertical displacement, and electrical resistance

Figures 8, 9, and 10 show the measured lateral force, loading force, and vertical displacement as the functions of sliding distance at various sliding speeds at 5, 55, and 95% RH respectively. To discuss the physical effect of the adsorbed water layer without the influences of the roughened surfaces, the main focus of this study is limited to the first half of the sliding where the roughening of the sliding surface is minimal. The increment of lateral force along the travel distance for all sliding speeds can be attributed to the increasing loading force [17], while the steepness of lateral force increment against the travel distance decreases when the sliding speed increases. At 5% RH, the change of slope for the lateral force is observed at the beginning of sliding and is retained longer at higher sliding speeds. This

is supposed to be caused by the compression of the ice-like water structure on the sliding interface. The adsorbed water layers exist in tetrahedral hydrogen-bonded ice-like structure which can grow up to three monolayers at RH below 30% [28]. Based on this, the authors proposed that as the low loading force increases, the ice-like water structure is disrupted and transformed into a liquid-like structure. This thin layer of liquid monolayers can provide minimal lubrication when the loading force is low. At high sliding speeds, the increased squeeze lubrication can enhance lubrication. For $20 \mu\text{m}\cdot\text{s}^{-1}$ (Fig. 8 (a)), the lateral force reaches the peak value at around $1500 \mu\text{m}$, where the loading force is also reaching 10 N at this point. The lateral force for $200 \mu\text{m}\cdot\text{s}^{-1}$ (Fig. 8 (b)) and $2000 \mu\text{m}\cdot\text{s}^{-1}$ (Fig. 8 (c)) reach the peak value at $2, 200,$ and $2800 \mu\text{m}$ respectively. For 55% RH, the trend of lateral force at 20 and $200 \mu\text{m}\cdot\text{s}^{-1}$ is fairly similar to 5% RH. Note that the discontinuity observed in 200 and $2000 \mu\text{m}\cdot\text{s}^{-1}$ for all RH is caused by the stick-slipping of the specimen, where

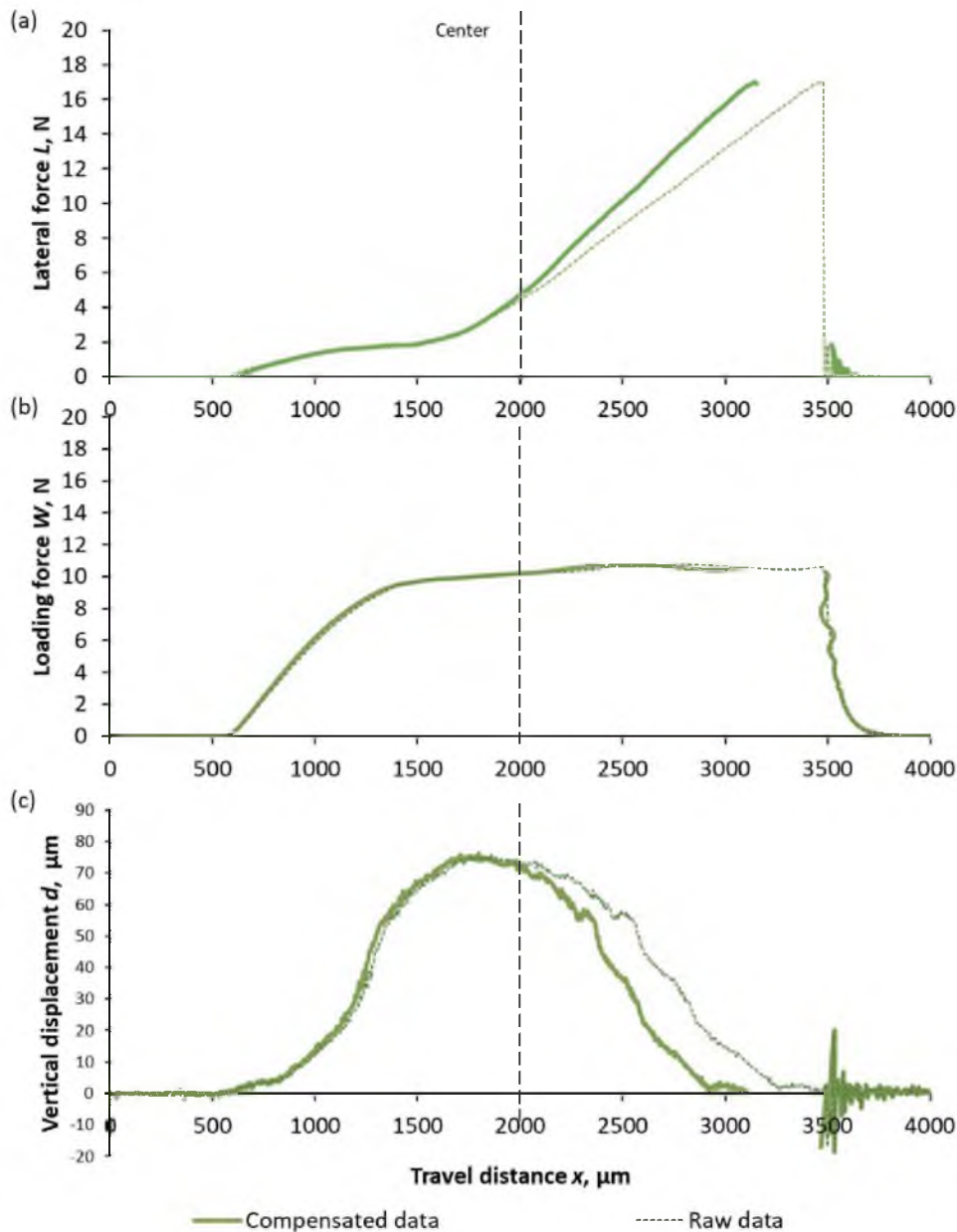


Fig. 6 Comparison of compensated and raw measurement at $2000 \mu\text{m}\cdot\text{s}^{-1}$ at 95% RH for (a) lateral force, (b) loading force, and (c) vertical displacement

the lateral force plunges abruptly. An interesting observation is that the lateral force for $2000 \mu\text{m}\cdot\text{s}^{-1}$ (Fig. 10 (c)) at 95% RH maintained below 2 N from 600 to 1500 μm for all repeated tests.

The trend of the loading force can be related to the lateral force. The loading force for all cases is increasing in the first half of sliding (600 to 2000 μm), while in the second half of sliding, the loading forces are decreasing for all cases except for $2000 \mu\text{m}\cdot\text{s}^{-1}$ at all RH. For $2000 \mu\text{m}\cdot\text{s}^{-1}$ at all RH, the loading force is increasing until the end of sliding then drops abruptly with some fluctuations, which can be related to the plunging of the high lateral force and the vibration of the measurement system due to the abrupt separation of the specimens. The discontinuity of loading force at 200 and $2000 \mu\text{m}\cdot\text{s}^{-1}$ is caused by the plunging of the high lateral force or 'slipping' of the specimens. Except at the point where the specimens are 'slipping', the upper

and lower specimens for all sliding conditions are maintained in good contact throughout the sliding as the loading force increases and decreases gradually without abrupt changes.

Generally, the vertical displacement plot for all cases increases in the first half of sliding, then decreases in the second half. Most of the tests have achieved the initial overlapping distance of 80 μm . Cases with displacement higher than the initial value are most probably caused by the build-up debris and the roughened surface during sliding. The same reason goes for the fluctuations observed especially for 5% RH, from the position where the lateral force is increasing steeply across the travel distance (from 700 ~ 1000 μm). It should be the position where the sliding interfaces start to roughen [16]. Compared to all the other cases, $2000 \mu\text{m}\cdot\text{s}^{-1}$ at 55 and 95% RH (Figs. 9 (c) and 10 (c)) has a smoother displacement plot when $x < 2000 \mu\text{m}$, due to the lubricative effect of the thick adsorbed water layer at high

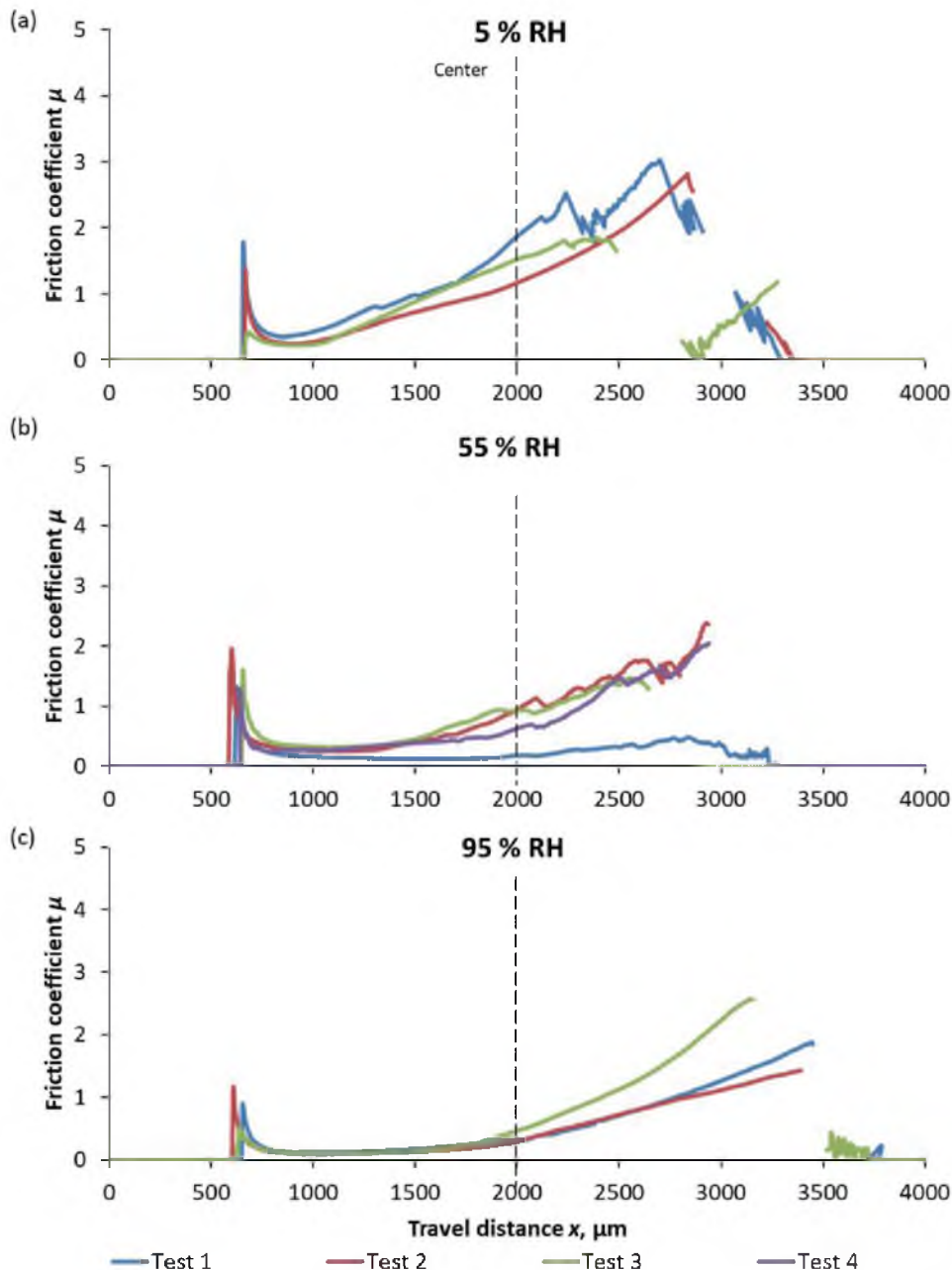


Fig. 7 Repeatability of friction coefficient for all 3 tests at $2000 \mu\text{m}\cdot\text{s}^{-1}$ for (a) 5%, (b) 55%, and (c) 95% RH

sliding speed. The fluctuations at the end of sliding observed in $2000 \mu\text{m}\cdot\text{s}^{-1}$ for all RH correspond to the observations in lateral force and loading force, which are caused by the vibration of the measurement system when the specimens are separated abruptly.

Figure 11 shows the electrical resistance of the sliding system for both RH. Overall, the specimens are expected to be fully conductive throughout the sliding if there is no physical separation between the metallic surfaces. However, for 55 and 95% RH, there are fluctuations observed at the beginning of sliding until $1000 \mu\text{m}$ at $2000 \mu\text{m}\cdot\text{s}^{-1}$. This indicates that the direct contact of the metallic surfaces is prevented by the thick adsorbed water layer and the squeeze lubrication by high sliding speed, which can be evidence of the physical lubrication effect by the adsorbed water layers.

3.4 Friction coefficient

The friction coefficient throughout the sliding contact at different sliding speeds for all RH deduced using formulae (1) to (4) from the experimental results is plotted in Fig. 12. The high friction coefficient at the beginning of sliding is caused by the very low normal force when the specimens are just approaching each other, which should be disregarded from the discussion. The adsorbed water layer under RH below 30% consists mainly of an ice-like water structure [28] with an estimated thickness of 1.76 nm (around 3 water monolayers), thus dry sliding is assumed for the case of 5% RH. While at 55% RH, the adsorbed water layers are estimated at 14 nm thick and are still dominantly in an ice-like form with less liquid structure [28]. At 95% RH, the maximum thickness of adsorbed water layer is considerably thick at 19 nm, consisting of around 63

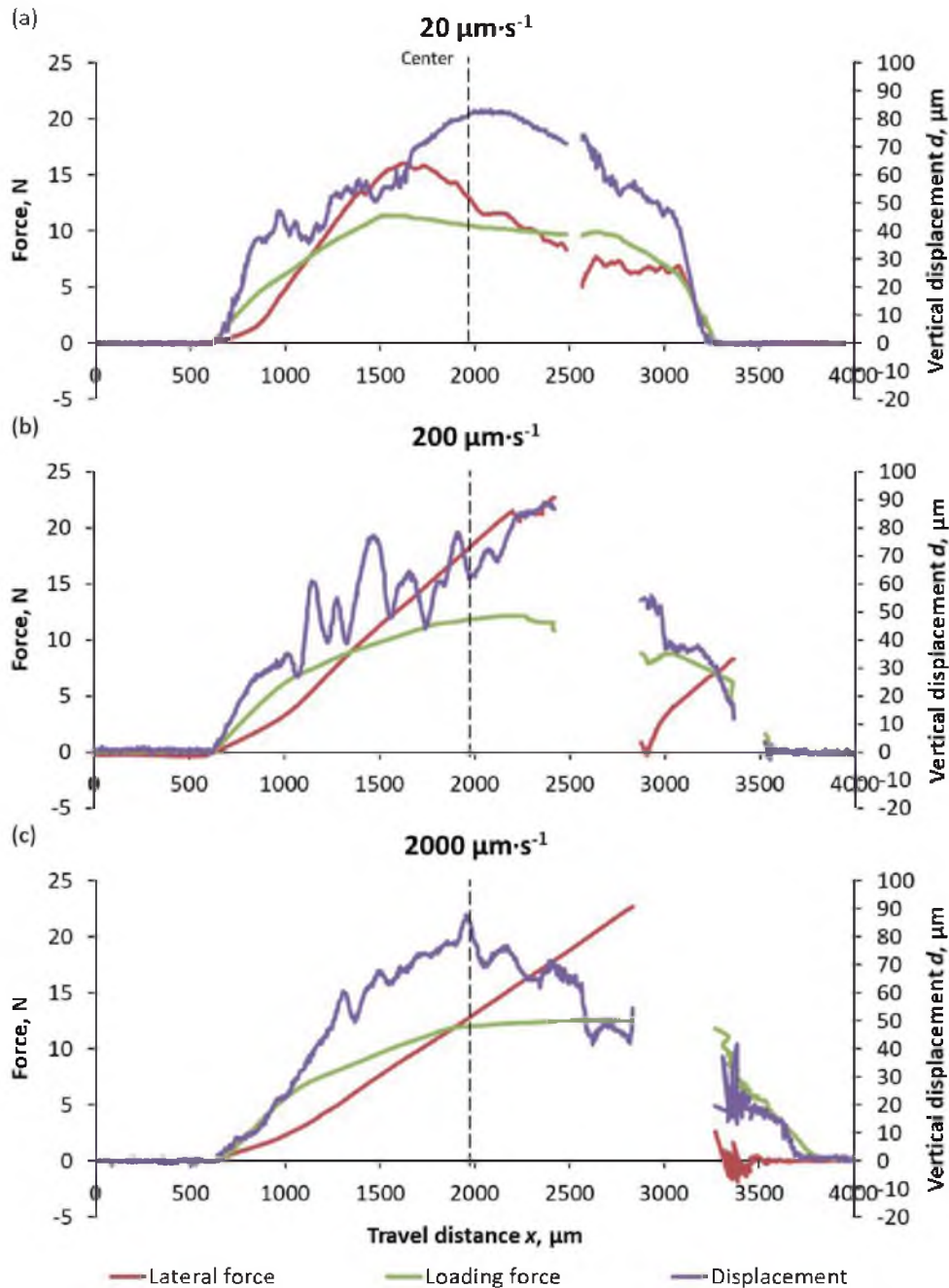


Fig. 8 Comparison of lateral force, loading force, and vertical displacement as a function of travel distance at (a) 20, (b) 200, and (c) 2000 $\mu\text{m}\cdot\text{s}^{-1}$ at 5% RH

water monolayers. For all RH, the friction coefficient in the first half of sliding is decreasing with increasing sliding speed. The trend of friction coefficient for 20 $\mu\text{m}\cdot\text{s}^{-1}$ at all RH shows that the physical effect of the adsorbed water layer is insignificant at a very low sliding speed. The authors suggested the possibility of squeezing out of the adsorbed water layer by the increasing loading force at a low sliding speed, which increases the solid-solid contact between the sliding interfaces [29]. From the beginning of sliding at 2000 $\mu\text{m}\cdot\text{s}^{-1}$, the friction coefficient is decreasing along the travel distance and is maintained low for some period for all RH, labeled as the effective lubricated region (ELR) in Fig. 9. The length of ELR is increasing with increasing RH%. Due to the thick adsorbed water layer, 95% RH has the

longest ELR around 800 μm ($600 < x < 1400 \mu\text{m}$), followed by RH%. 55 around 600 μm ($600 < x < 1200 \mu\text{m}$). 5% RH has the shortest ELR of 360 μm ($600 < x < 960 \mu\text{m}$). The decreasing friction coefficient for 55 and 95% RH corresponds to the fluctuating contact resistance in Figs. 11 (b) and (c), where the adsorbed water layers physically separate the sliding interfaces. The difference in ELR at different RH can be attributed to the less direct contact between the asperities at higher RH due to the thicker adsorbed water on the specimen surfaces acting as a lubricant [25]. Another interesting point observed in high sliding speed at 95% RH is that the friction coefficient is maintained as low as 0.1 in the ELR, corresponding to the value of friction coefficient for boundary lubrication in the Stribeck

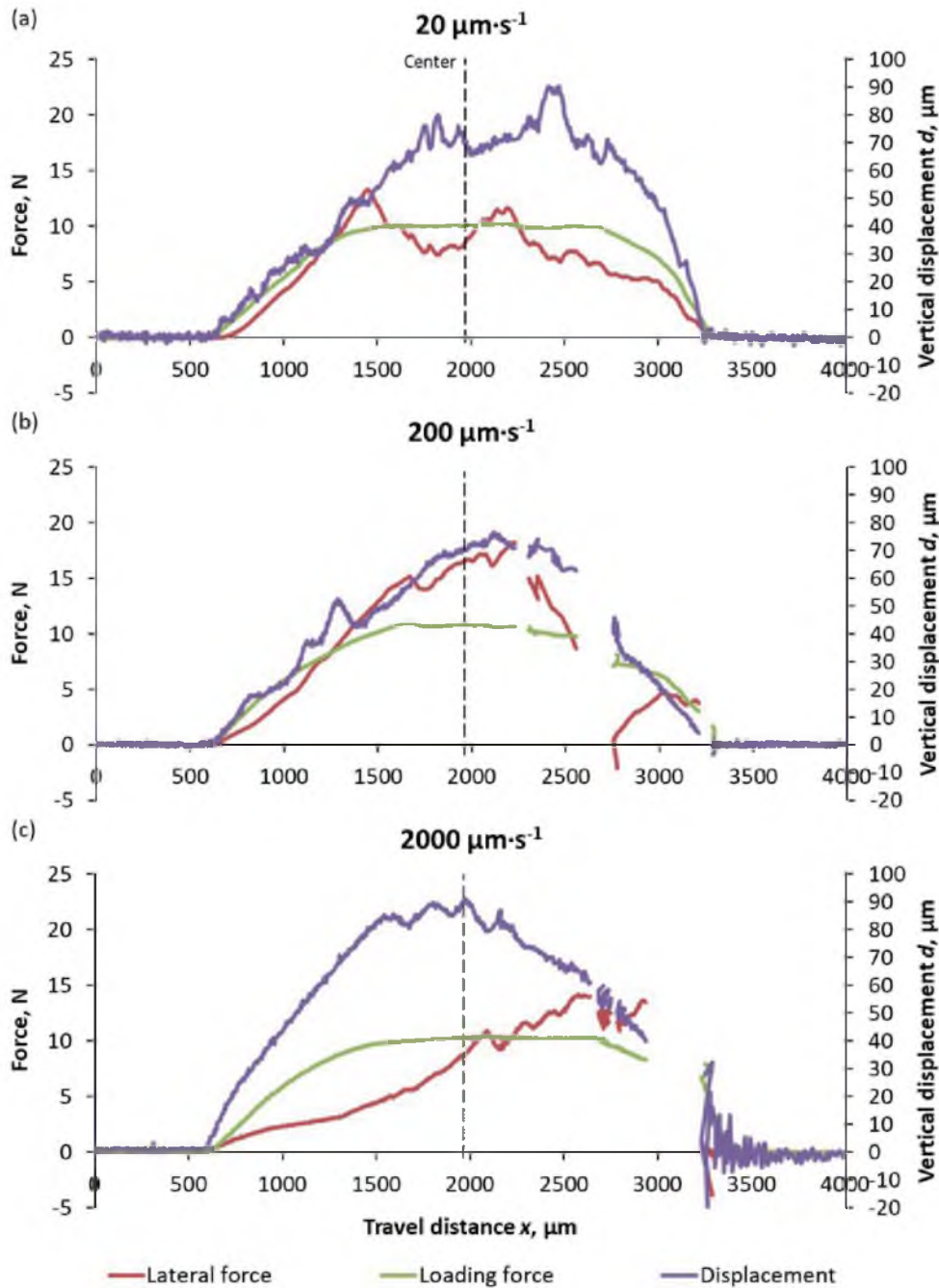


Fig. 9 Comparison of lateral force, loading force, and vertical displacement as a function of travel distance at (a) 20, (b) 200, and (c) 2000 $\mu\text{m}\cdot\text{s}^{-1}$ at 55% RH

curve. For this, the authors proposed that the low loading force and high sliding speed might enable the wedging lubricating effect of the thick adsorbed water layer, effectively preventing solid-solid interaction between the sliding interfaces before the loading force reaches 10 N. Once the loading force starts to stabilize and decreases, the adsorbed water layer between the sliding interfaces might be squeezed out, causing an increase in solid-solid interaction after 1500 μm , which increases the real contact area. For 20 $\mu\text{m}\cdot\text{s}^{-1}$, the sliding phenomena should be mainly governed by the surface roughness of the sliding interfaces.

Figure 13 shows the average friction coefficient as a

function of sliding speed in the first half of sliding ($800 \mu\text{m} < x < 1500 \mu\text{m}$) at all RH. The average friction coefficient from 1500 μm onwards is more complex to be summarized graphically due to the roughened sliding interfaces, thus only the range of friction coefficient before the surface roughening starts is considered in the discussion. The average friction coefficient is decreasing with increasing sliding speed at all RH. The friction coefficient for 5% RH decreases gradually from 0.9 to 0.67 with increasing sliding speed from 20 to 2000 $\mu\text{m}\cdot\text{s}^{-1}$. The friction coefficient for 55% RH decreases gradually from 0.81 to 0.69 for a sliding speed of 20 to 200 $\mu\text{m}\cdot\text{s}^{-1}$, then drops significantly to 0.36 when the sliding speed reaches 2000 $\mu\text{m}\cdot\text{s}^{-1}$. For 95% RH,

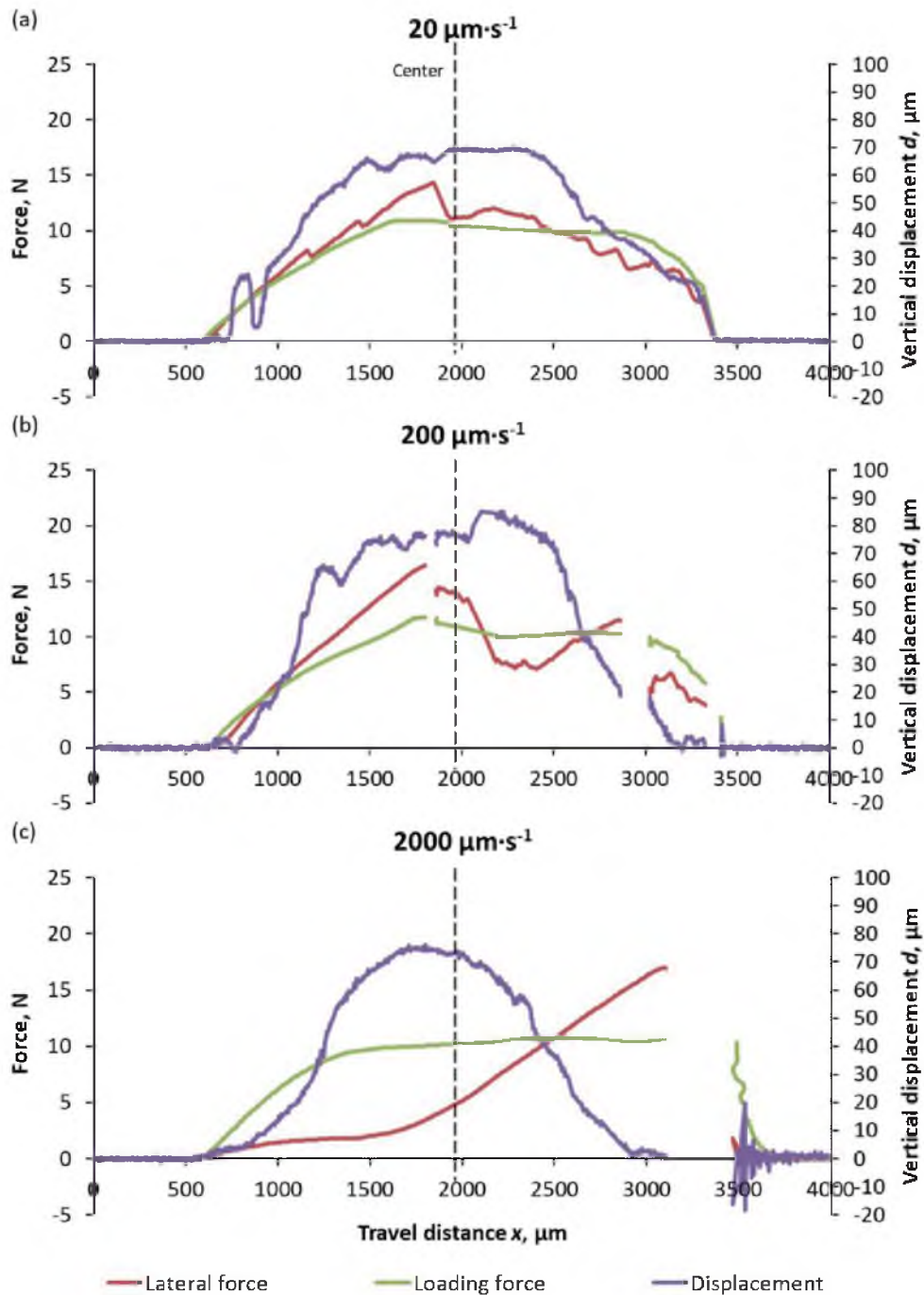


Fig. 10 Comparison of lateral force, loading force, and vertical displacement as a function of travel distance at (a) 20, (b) 200, and (c) 2000 $\mu\text{m}\cdot\text{s}^{-1}$ at 95% RH

the friction coefficient decreases with a similar trend as 55% RH, which first decreases gradually from 0.64 to 0.54 and then drops to 0.13. The almost parallel decreasing trend of friction coefficient for all conditions except 2000 $\mu\text{m}\cdot\text{s}^{-1}$ at 55 and 95% RH can be associated with the typical friction-velocity curve widely recognized for dry sliding, where the friction coefficient decreases at a factor of 2 with sliding speed increasing at a factor of 10 [30]. The additional decrease in friction coefficient for 2000 $\mu\text{m}\cdot\text{s}^{-1}$ at 55 and 95% RH should be attributed to the physical lubrication of the adsorbed water layers. From the results, the high value of friction coefficient observed for all sliding conditions is typical for dry sliding except for 2000

$\mu\text{m}\cdot\text{s}^{-1}$ at 95% RH. The lowest friction coefficient at 95% RH can reach 0.1 when the sliding speed increases reaches 2000 $\mu\text{m}\cdot\text{s}^{-1}$, indicating the possibility of achieving boundary lubrication at such conditions. It is worth noting that the standard deviation of the average friction coefficient for the repeated tests at each sliding condition is significantly lower for 2000 $\mu\text{m}\cdot\text{s}^{-1}$ at 95% RH, while the other combinations of conditions have a higher standard deviation. This could be evidence of the liquid lubrication effect of 2000 $\mu\text{m}\cdot\text{s}^{-1}$ at 95% RH. Liquid-mediated sliding is much more stable and will produce less variety of data, thus the higher repeatability for 2000 $\mu\text{m}\cdot\text{s}^{-1}$ at 95% RH. On the other hand, dry sliding tends to produce fluctuating and

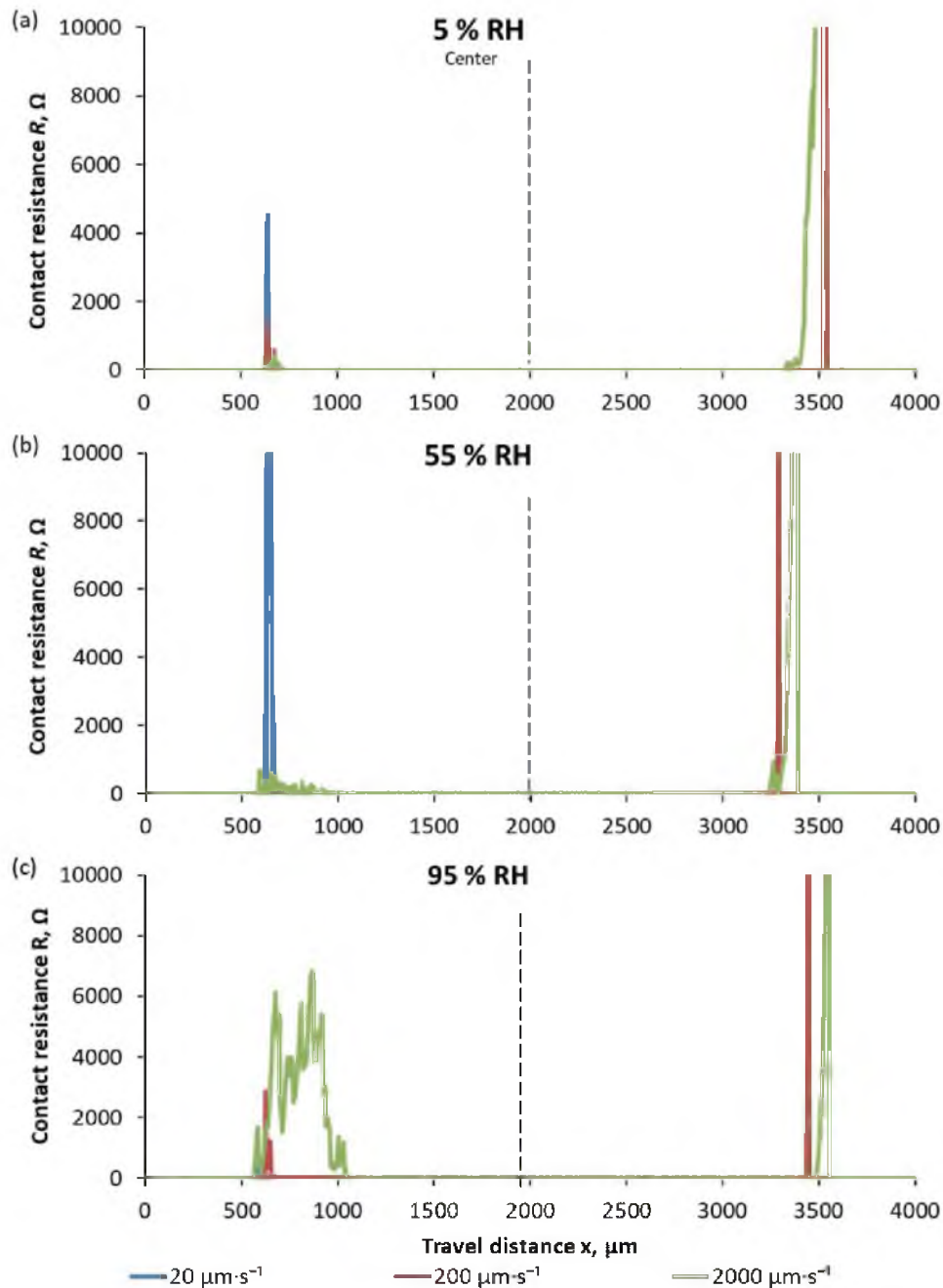


Fig. 11 Electrical resistance as a function of travel distance at 20, 200, and 2000 $\mu\text{m}\cdot\text{s}^{-1}$ for (a) 5%, (b) 55%, and (c) 95% RH

high range of friction coefficients due to the solid-solid contact being the major component governing the sliding phenomena. A previous study using the same conditions and tribotester also reported a similar observation where low to medium RH shows a larger variety of data [23]. Thus, the friction coefficient will have a larger range of values for all conditions except for 2000 $\mu\text{m}\cdot\text{s}^{-1}$ at 95% RH.

3.5 Surface roughness of wear track

The average wear depth at various positions on the wear track of the upper ball specimen is plotted in Fig. 14. The average wear depth at 5 positions including the center slice (950 μm) is measured and plotted against the wear track. Overall, the peak value of wear depth at all RH is decreasing with increasing the

sliding speed at all RH. The distribution of the wear depth values complements the fluctuations of the vertical displacement plot in Figs. 8, 9, and 10, in which the region with fluctuating vertical displacement has higher wear depth. Generally, the wear depths before 1000 μm for 2000 $\mu\text{m}\cdot\text{s}^{-1}$ at 95% RH are very low compared to the other sliding conditions. This could also be evidence of the liquid lubrication effect at high RH and sliding speed.

4 Conclusion

By examining the friction coefficient variation with sliding speed and RH, the friction coefficient decreases significantly when sliding speed increases to 2000 $\mu\text{m}\cdot\text{s}^{-1}$ at 55 and 95% RH, while the decrease of friction coefficient for other conditions

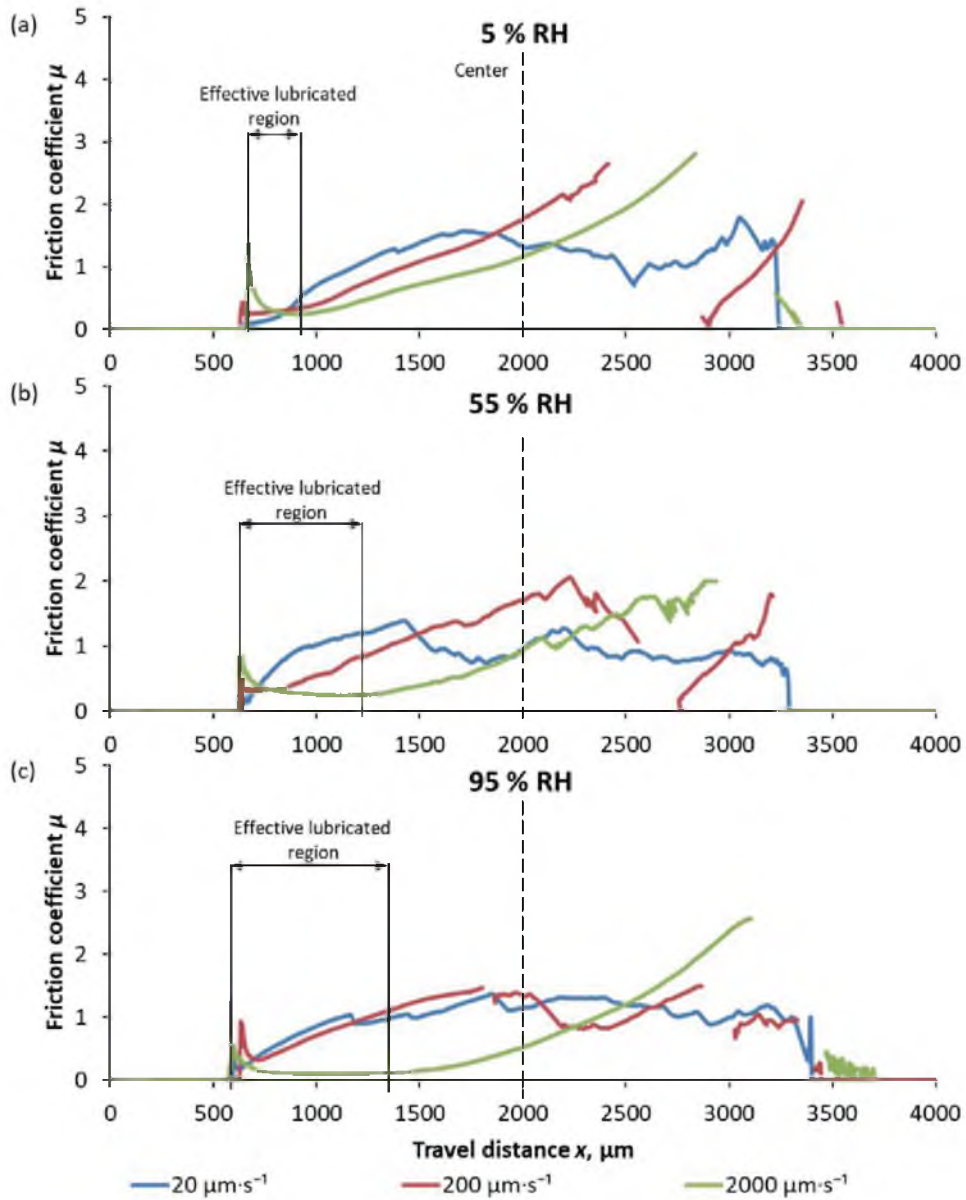


Fig. 12 Friction coefficient as a function of travel distance at 20, 200, and 2000 $\mu\text{m}\cdot\text{s}^{-1}$ for (a) 5%, (b) 55%, and (c) 95% RH

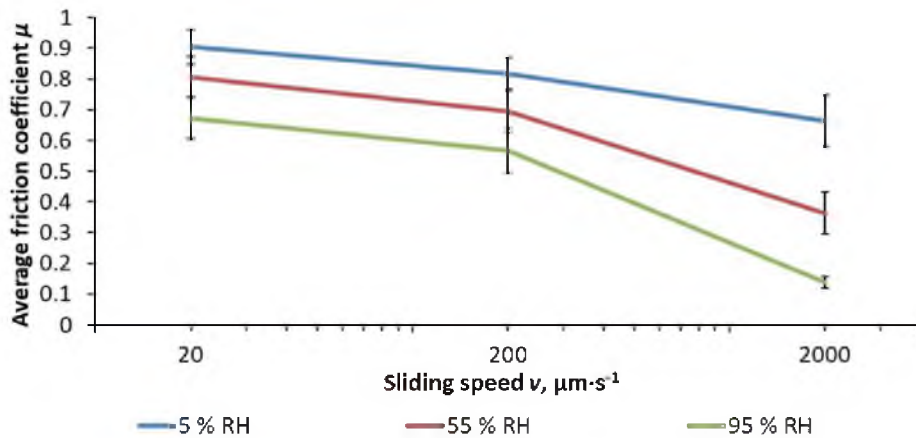


Fig. 13 Average friction coefficient ($800 \mu\text{m} < x < 1500 \mu\text{m}$) as a function of sliding speed for 3 tests at 5, 55, and 95% RH

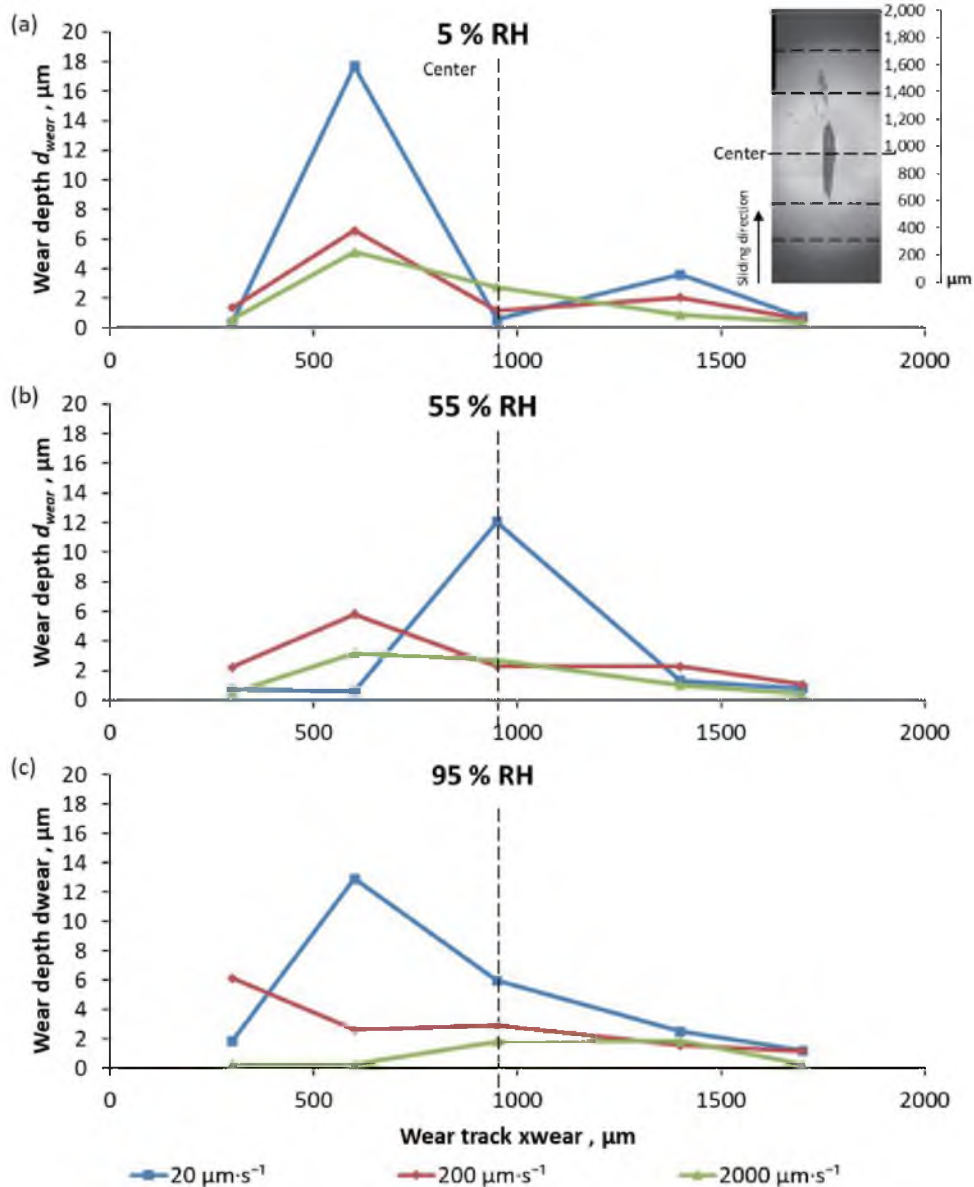


Fig. 14 Average wear depth at various positions of wear track for the upper ball specimen at 20, 200, and 2000 $\mu\text{m}\cdot\text{s}^{-1}$ for (a) 5%, (b) 55%, and (c) 95% RH

remained low, which corresponds to the widely known phenomena for non-lubricated sliding of materials [30]. Dry sliding phenomena were expected for all conditions except $2000 \mu\text{m}\cdot\text{s}^{-1}$ at 95% RH, as the adsorbed water layer mostly exists in an ice-like structure. At very low sliding speeds, the sliding phenomena are mainly governed by the surface condition of the sliding interfaces regardless of the RH.

Evidence suggested the physical lubrication effect of the adsorbed water layers at $2000 \mu\text{m}\cdot\text{s}^{-1}$ at 55 and 95% RH:

1. The high contact resistance at the beginning of sliding indicates the physical separation of the metallic surfaces by the adsorbed water layers.
2. The additional decrease of friction coefficient for $2000 \mu\text{m}\cdot\text{s}^{-1}$ at 55 and 95% RH can be related to the physical lubrication effect of the adsorbed water layers.
3. The friction coefficient for $2000 \mu\text{m}\cdot\text{s}^{-1}$ at 95% RH reached as low as 0.1, which falls into the boundary lubrication of the Stribeck curve.
4. Wear depths before 1000 μm for $2000 \mu\text{m}\cdot\text{s}^{-1}$ at 95% RH is very low compared to other conditions, indicating the prevention of surface roughening by the adsorbed water layers.

References

- [1] Goto H, Buckley DH. The influence of water vapour in air on the friction behaviour of pure metals during fretting. *Tribology International*. 1985;18(4): 237-245.
- [2] Fukuda K, Norose S, Sasada T. Effect of humidity on sliding wear in Fe and Cu rubbing system. *Proceedings of the Japan Congress on Materials Research*. 1985;28: 89-92.
- [3] Sasaki S. The effects of the surrounding atmosphere on the friction and wear of alumina, zirconia, silicon carbide and silicon nitride. *Wear*. 1989;134(1): 185-200.
- [4] Lancaster JK. A review of the influence of environmental humidity and water on friction, lubrication and wear. *Tribology International*.

- 1990;23(6): 371-389.
- [5] Buckley DH. The metal-to-metal interface and its effect on adhesion and friction. *Journal of Colloid and Interface Science*. 1977;58(1): 36-53.
- [6] Liew WYH. Effect of relative humidity on the unlubricated wear of metals. *Wear*. 2006;260(7-8): 720-727.
- [7] Asaduzzaman CM, Helali M. The effect of relative humidity and roughness on the friction coefficient under horizontal vibration. *The Open Mechanical Engineering Journal*. 2008;2(1): 128-135.
- [8] Chowdhury MA, Nuruzzama DM, Hannan A. Effect of sliding velocity and relative humidity on friction coefficient of brass sliding against different steel counterfaces. *International Journal of Engineering Research and Applications*. 2012;2(2): 1425-1431.
- [9] Klaffke D. On the repeatability of friction and wear results and on the influence of humidity in oscillating sliding tests of steel-steel pairings. *Wear*. 1995;189(1-2): 117-121.
- [10] Bregliozzi G, Di Schino A, Kenny JM, Haefke H. The influence of atmospheric humidity and grain size on the friction and wear of AISI 304 austenitic stainless steel. *Materials Letters*. 2003;57(29): 4505-4508.
- [11] Masuko M, Aoki S, Suzuki A. Influence of lubricant additive and surface texture on the sliding friction characteristics of steel under varying speeds ranging from ultralow to moderate. *Tribology Transactions*. 2005;48(3): 289-298.
- [12] Binggeli M, Mate CM. Influence of capillary condensation of water on nanotribology studied by force microscopy. *Applied Physics Letters*. 1994;65(4): 415-417.
- [13] Ando Y. The effect of relative humidity on friction and pull-off forces measured on submicron-size asperity arrays. *Wear*. 2000;238(1): 12-19.
- [14] Feiler AA, Jenkins P, Rutland MW. Effect of relative humidity on adhesion and frictional properties of micro- and nano-scopic contacts. *Journal of Adhesion Science and Technology*. 2005;19(3-5): 165-179.
- [15] Subhi ZA, Morita T, Fukuda K. Analysis of humidity effects on early stage of sliding. *Procedia Engineering*. 2013;68: 199-204.
- [16] Fukuda K, Subhi ZA, Morita T. Analytical study on the growth and transfer of adhesive substances generated on the surface in the early stage of sliding. *Wear*. 2015;330-331: 64-69.
- [17] Subhi ZA, Fukuda K, Morita T, Sugimura J. Analysis on the mechanism of humidity to influence the very early stage of sliding under different load. *Tribology Online*. 2015;10(6): 420-427.
- [18] Fukuda K, Morita T. Physical model of adhesive wear in early stage of sliding. *Wear*. 2017;376-377: 1528-1533.
- [19] Subhi ZA, Fukuda K. Influences of atmospheric humidity on the adhesion mechanisms of brass and austenitic stainless steel. In *Proceedings of JAST Tribology Conference Niigata*. 2016.
- [20] Subhi ZA, Fukuda K. Analysis on the early stage of contact adhesion in different relative humidity. In *Malaysia-Japan Joint International Conference 2016*. Kuala Lumpur, Malaysia. 2016.
- [21] Subhi ZA, Fukuda K. Adhesion of polytetrafluoroethylene (PTFE) on austenitic stainless steel (JIS SUS316) during the initial stage of sliding at different atmospheric humidity. In *5th Malaysia-Japan Tribology Symposium 2017*. Kuala Lumpur, Malaysia. 2017.
- [22] Yap KK, Fukuda K, Subhi ZA. Effects of adsorbed water due to atmospheric humidity on ball-to-ball sliding contact. *Proceedings of Asia International Conference on Tribology 2018*. 2018: 169-170.
- [23] Fukuda K, Sheng SL, Subhi ZA. Tribological behavior of hydrophilic and hydrophobic surfaces in atmosphere with different relative humidity. *Tribology Online*. 2019;14(5): 353-358.
- [24] Manaf NDA, Fukuda K, Subhi ZA, Radzi MFM. Influences of surface roughness on the water adsorption on austenitic stainless steel. *Tribology International*. 2019;136: 75-81.
- [25] Subhi ZA, Fukuda K, Morita T, Sugimura J. Quantitative estimation of adsorbed water layer on austenitic stainless steel. *Tribology Online*. 2015;10(5): 314-319.
- [26] Fukuda K. Friction force distribution and its alternation with repeated sliding. *Journal of Japanese Society of Tribologists*. 1998;43(9): 788-795 (in Japanese).
- [27] Fukuda K. Analysis of specimen displacement in repeated sliding system. *Journal of Japanese Society of Tribologists*. 2004;49(9): 738-745 (in Japanese).
- [28] Asay DB, Kim SH. Evolution of the adsorbed water layer structure on silicon oxide at room temperature. *The Journal of Physical Chemistry B*. 2005;109(35): 16760-16763.
- [29] Khan SH, Hoffmann PM. Squeeze-out dynamics of nanoconfined water: A detailed nanomechanical study. *Physical Review E*. 2015;92(4): 042403.
- [30] Rabinowicz E, Tanner R. Friction and wear of materials. *Journal of Applied Mechanics*. 1966;33(2): 479.



This paper is licensed under the Creative Commons Attribution-NonCommercial-NoDerivatives 4.0 International (CC BY-NC-ND 4.0) License. This allows users to copy and distribute the paper, only upon conditions that (i) users do not copy or distribute such paper for commercial purposes, (ii) users do not change, modify or edit such paper in any way, (iii) users give appropriate credit (with a link to the formal publication through the relevant DOI (Digital Object Identifier)) and provide a link to this license, and (iv) users acknowledge and agree that users and their use of such paper are not connected with, or sponsored, endorsed, or granted official status by the Licensor (i.e. Japanese Society of Tribologists). To view this license, go to <https://creativecommons.org/licenses/by-nc-nd/4.0/>. Be noted that the third-party materials in this article are not included in the Creative Commons license, if indicated on the material's credit line. The users must obtain the permission of the copyright holder and use the third-party materials in accordance with the rule specified by the copyright holder.